中國機械工程學刊第四十二卷第一期第 81~91 頁(民國一百一十年)
Journal of the Chinese Society of Mechanical Engineers, Vol.42, No.1, pp 81~91 (2021)

Development of a Multilayered Magnetorheological Brake for Knee Orthosis Applications

Yaojung Shiao*, Thang Hoang**, Mahendra Babu Kantipudi**, Nung-Chin Kao*** and Chien-Hung Lai ****

Keywords: magneto-rheological (MR) fluid, knee orthosis, MR brake, multilayer

ABSTRACT

Traditional passive knee orthoses support patients to walk. However, they cannot enable patients achieve a regular walking rhythm. Conventional active knee orthoses (AKOs) can apply motors to help patients walk smoothly; however, their heavy weight, high cost, and high power consumption are not suitable for most consumers. This study developed a novel multilayer magnetorheological (MR) brake (MRB) for knee orthoses with variable resistance. This MRB overcomes the drawbacks of conventional knee orthoses and motor-driven AKOs. The MRB primarily comprises a rotor, stator, and single magnetic pole and MR layers. The rotor and stator have multiple discs; both sides of the discs are surrounded by MR fluid layers. This multilayer structure provides a relatively high torque density during braking. The proposed brake was optimized through electromagnetic simulations. Subsequently, an MRB prototype was fabricated, and its performance characteristics were experimentally examined to confirm the design requirements. The results showed that the proposed MRB achieved a torque and torque–volume ratio (TVR) of 12.5 N·m and 46 N·m/dm^3, respectively. Because of the high TVR, this brake is more suitable than existing MRBs in AKO applications. Additionally, this brake exhibits advantages of rapid response (response time: 170 ms), easy control, low weight, and low power consumption.

Paper Received April, 2020. Revised July, 2020. Accepted August, 2020. Author for Correspondence: Chien-Hung Lai

* *Professor, Dept. of Vehicle Engineering, National Taipei University of Technology, Taiwan.*

** *Ph.D. student, Dept. of Vehicle Engineering, National Taipei University of Technology, Taiwan.*

*** *Graduate student, Dept. of Vehicle Engineering, National Taipei University of Technology, Taiwan.*

**** *Dept. of Physical Medicine and Rehabilitation, School of Medicine, College of Medicine, Taipei Medical University, Taiwan.*

**** *Dept. of Physical Medicine and Rehabilitation, Taipei Medical University Hospital, Taiwan.*

Author for Correspondence: Chien-Hung Lai, Tel: 886-2-27372181 ext. 3538, Email: chlai@tmu.edu.tw

INTRODUCTION

Loss of leg mobility is becoming a common problem that can be attributed to the increasing occurrence of spinal cord injury, brain malfunction, and muscle weakness. Consequently, many patients experience gait abnormalities characterized by symptoms such as walking difficulty or frequent falling. Such patients require walking aids to restore leg mobility. Currently, conventional knee orthoses (CKOs) are commonly used aid devices. Although CKOs are cheap and highly durable, variations in their functioning are considerably limited (Ahmadkhanlou et al., 2007). Specifically, the function knee aid devices must be customizable according to symptoms, leg size differences, and leg control factors, which cannot be achieved using CKOs. Therefore, developing multifunctional knee braces with an actively variable force (active knee orthoses, AKOs) is imperative. Pratt et al. (2004) designed a knee exoskeleton, namely RoboKnee, to enhance the strength and endurance of the user's knee during walking and to support the leg when climbing steps. Beyl et al. (2007) introduced an AKO with electric motors and pneumatic artificial muscles for gait rehabilitation. Banala et al. (2007) developed a motor-based powered leg orthosis for gait rehabilitation. Josep et al. (2011) modeled a new active stance-control knee-ankle-foot orthosis driven by a dc motor. Although these conventional motor-based AKOs provide active functions, their disadvantages comprise their relatively large size, heavy weight, and high power consumption (Dollar et al., 2007). Recently, semi-AKOs that can overcome the limitations of CKOs and the few limitations of AKOs have been introduced (Weinberg et al., 2007). Conceptual semiactive resistance devices currently used in knee orthoses can be categorized into two types: electrorheological (ER) and magnetorheological (MR) fluid (MRF)-based resistance devices. The size, weight, and power consumption of MRF devices are smaller than those of ER fluid-based devices.

MRF is a smart material for engineering applications. Rabinow (1948) and Rosensweig et al. (1968) have discussed this controllable fluid. This fluid is a mixture of micron-sized ferromagnetic particles and carrier fluid such as silicon or mineral oil. When the MRF is exposed to a magnetic field, the ferromagnetic particles suspended in the fluid exhibit a chain structure oriented in the direction parallel to the magnetic field (Fig. 1). The chain structure increases the viscosity of the fluid and then engenders increased shear stress. If the external magnetic field increases, the shear strength of the fluid increases, resulting in a fluid-like solid. If the magnetic field is removed, the fluid-like solid is reverted to its liquid state. The time required for these reactions is only a few milliseconds. The advantages of this MR technology are rapid response, low noise, low energy consumption, and high controllability.

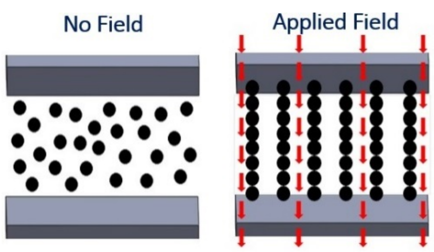

Fig. 1. Response of MRF particles to the applied magnetic field.

The application of MRF can be divided into three modes: flow, direct-shear, and squeeze modes. In the first mode, MRF resists flow between two stationary objects because of the MR effect [Fig. 2(a)]. This resistance mode is useful in devices operating in flow mode, such as dampers, shock absorbers, and valves. In the second mode, the fluid resists the relative motion between two objects [Fig. 2(b)]. This resistance mode can be used to design MR brakes (MRBs) and clutches. In the third mode, MRF can resist an applied compressive force; it is thus useful in devices operating in squeeze mode, including engine mounts and haptic black boxes. Fig. 2(c) illustrates the magnetic field and fluid motion direction in the squeeze mode.

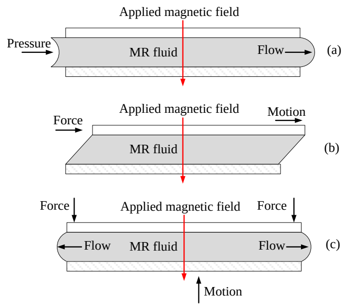

Fig. 2. Operating modes of MRF (Shiao et al., 2013).

MRB technology is the most suitable alternative for conventional prosthetic devices (Carlson et al., 2001). Several MRF-based devices have already been developed for knee orthosis applications (Gao et al., 2017; Arteaga et al., 2020; Ma et al., 2017;Takesue et al., 2000) Ar. An MRB is a device providing a controllable resistance force to the setup of an orthopedic active knee brace. Ahmad et al. (2007) explained the use of an MRB in an AKO. The maximum torque generated by this MRB was determined to be 6 N·m at an applied coil current of 4 A. Li et al. (2006) established an MRB for AKOs that can be applied to ankle joints to enable individuals to walk smoothly. However, for practical use of this device, further investigation is required. Therefore, the main objective of this study was to develop a controllable, small-volume, high-torque, and rapid response MRF-based brake for AKO applications.

A basic MRB comprises a rotor, a stator, and MRF layers. The shear resistance of the MRF can be adjusted by changing the strength of the magnetic field in the core. An MRB can be classified as a disc-type or drum-type MRB according to the rotor geometry. In a disc-type MRB, the rotor is a thin and circular disc and is surrounded by MRF. When the magnetic field is activated, the MRF around the disc attains a chain structure and exerts a resistance force on disc faces. This type of MRB is useful for devices with a thin accessible space. By contrast, in a drum-type MRB, the rotor is a long cylindrical drum with considerable width, and a magnetic field flux is applied to the MRF in the radial direction. This MRB is useful for applications with long cylindrical space. Another type of MRB design is a T-type hybrid brake, which is a combination of disc-type and drum-type MRBs. It provides higher torque than that provided by disc-type and drum-type brakes (Nguyen et al., 2012, 2015).

LORD Corporation designed and manufactured the first simple single-disc brake with a maximum resistance of 4 N·m. Attia et al. (2017) investigated the performance of this brake theoretically and experimentally. Li and Du (2003) introduced a disc-shaped MRB design with a simple disc construction. As observed in these studies, the braking torque increases progressively with the magnetic field or rotational speed. However, when the magnetic field reaches its saturation limit, the torque does not increase further. This torque point is called the maximum torque. The maximum torque generated by the aforementioned single-disc brake designs is considerably low. Zhou et al. (2007) developed an MRF-based brake with two shearing discs. Wang et al. (2013) designed a multidisc MRB with eight disc layers. In these multilayer MRF-based brakes, the braking torque is significantly higher than that in single-layer MRF-based brakes. Increasing the number of layers increases the contact area between the rotor and MRF, thus increasing the torque substantially. However, this design also increases the overall size and weight of brakes. Therefore, designing a brake that can effectively achieve a high torque–volume ratio (TVR) is crucial.

Shiao and Nguyen (2013) designed a novel multipole MRB to effectively utilize the available magnetic field to generate a high braking effect on the rotor surface. This multipole MRB contains multiple electromagnetic poles around a drum-type brake. Consequently, the active chaining areas for the MRF increase substantially, and the braking torque improves considerably. This multipole design not only uses the rotor area effectively but also improves the TVR of the brake considerably. Shiao also developed a new MRB with a combination of multiple electromagnetic poles and bilayer MR layers. The brake comprises two rotors situated outside and inside a six-pole stator. Therefore, this MRB can provide a higher torque and larger TVR than conventional single-layer or multipole MRBs can (Shiao et al., 2016). Recently, Wu et al. (2018) presented a radial multipole and multidrum MRB that can achieve high torque density. However, this model employs inner and outer poles to achieve the multipole concept. The applied poles occupy considerable volume, resulting in a decrease in the overall TVR. Furthermore, because of the occupation of outer poles, the brake cannot achieve a mechanical advantage; that is, the perpendicular distance from the MR layers to the center of the brake is relatively short. Moreover, all these brakes are not suitable for knee orthosis applications because of their complexity and drum brake structure (large brake width is required). Therefore, this study focused on the development of a thin MRB for orthosis applications. The design for this brake involved a disc-type structure, multilayer construction, and a single-pole magnetic field to achieve a thin size, high TVR, and simple assembly, respectively. Electromagnetic simulations were performed to optimize the brake design, and experimental tests were conducted to analyze the real-time response of the brake.

DESIGN OF MULTILAYER MRB

A compact multilayer and lightweight MRB with a simple disc construction was designed. Fig. 3 presents the cross-sectional view of the multilayer MRB. The MRB comprises several rotor plates, stator plates, and MRF layers. The stator has a cylindrical core surface, magnetic flux passage channels, and stator plates. The rotor is a hollow cylinder with internal plates. These internal plates are placed between the stator plates in series. The gaps between the rotor and stator plates are filled with MRF. MRF-140CG (LORD Corp.), a prominent and high-quality MRF, was selected for this brake. The viscosity and density of this fluid are 0.280 Pa·s and 3.54–3.74 g/cm^3, respectively. LORD Corp. provided the BH curve, yield stress, and other properties of the fluid (Data, 2008). The entire unit is enclosed with aluminum covers.

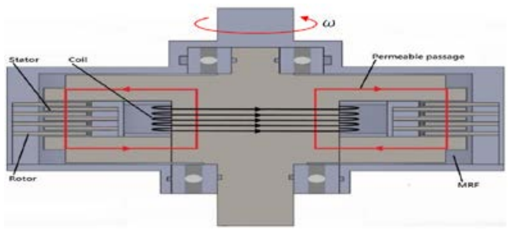

Fig. 3. Sectional view of multilayered MRB.

When a current passes through the coils, a magnetic field is generated in the stator core according to Ampere's right-hand rule. The magnetic flux passes through magnetically permeable materials—namely the stator passage channel, stator plates, and rotor plates—and then through the stator channel to form a closed magnetic loop. Fig. 3 illustrates the direction and loops of the magnetic field. Because of the magnetic field between the rotor and stator blades, particles suspended in the MRF exhibit a chain structure in the direction parallel to the magnetic field; thus, shear stress is established in the MRF. This shear stress provides the braking torque on the rotor blades. The torque (T_{MR}) depends on the magnetic field intensity and design parameters, as indicated in Eq (1):

$$T_{MR} = \int_{A_w}^{1} r\tau \, \mathrm{d}A_w, \qquad (1)$$

where τ is the total shear stress from the MRF. According to the Bingham plastic model, τ can be expressed as shown in Eq. (2):

$$\tau = \tau_{yd} + \eta \frac{\omega r}{g}, \qquad (2)$$

where A_w is the contact area of the MRF, r is the radius of the rotor, τ_{yd} is the yield shear stress due to the magnetic field, η is the MRF viscosity, ω is the angular velocity, and g is the MR layer thickness.

T_{MR} can be classified as indicated in Eq. (3).

$$T_{MR} = T_{yd} + T_{vis}\ , \qquad (3)$$

where T_{yd} is the yield torque, presented in Eq. (4), and T_{vis} is the viscous torque, presented in Eq. (5).

$$T_{yd} = \int_{r_1}^{r_2} \int_0^{2\pi} r^2 \, \tau_{yd} \, d\theta \, dr, \qquad (4)$$

$$T_{vis} = \eta \frac{\omega}{g} \int_{r_1}^{r_2} \int_0^{2\pi} r^3 \, d\theta \, dr. \qquad (5)$$

The total torque of the brake is expressed in Eq. (6):

$$T = T_{yd} + T_{vis} + T_{fr}, \qquad (6)$$

where T_{fr} is the frictional torque.

Finally, the total torque from the designed eight-layer MRB is provided in Eq. (7):

$$T_{total} = 8 \cdot [T_{yd} + T_{vis}] + T_{fr} = 8 \cdot [\tfrac{2}{3}\pi\tau_{yd} \cdot ({r_2}^3 - {r_1}^3) + \frac{\eta\pi\omega}{2g} \cdot ({r_2}^4 - {r_1}^4)] + T_{fr}. \qquad (7)$$

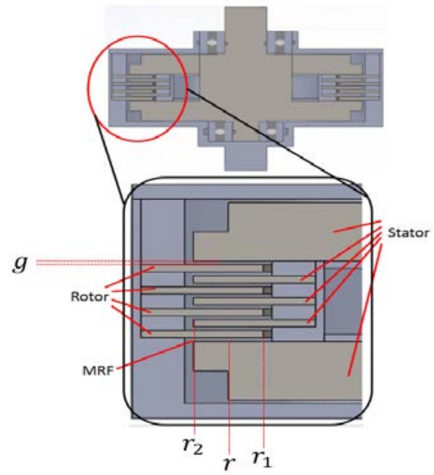

Fig. 4. Sectional view of the multilayer stator and rotor plates.

DESIGN OPTIMIZATION

Because the target application of the proposed multilayer MRB is for knee orthoses, the maximum permissible diameter and thickness of the brake are 96 and 35 mm, respectively. Accordingly, the MRB assembly must be confined within these size limits. During the design of the proposed MRB, this study first considered the MRF thickness. As presented in Eqs. (1) and (2), a thinner MRF layer can engender a higher braking torque. However, if the MRF layer is excessively thin, direct contact between the plates may induce a brake jam. Thus, this study applied a minimum thickness of 0.5 mm in the design. Subsequently, the study considered the thickness of the stator and rotor plates. Concerning the manufacturability and structural strength of the proposed brake, this study considered a least possible thickness of 1 mm. After considering allowances for the housing and assembly components of the MRB with respect to the specified thickness, this study determined that the plates and MR layers must be placed within a space of 11 mm. Accordingly, the proposed brake was constructed with a four-layer rotor, eight layers of MRF, and a five-layer stator. The second column of Table 1 presents the dimensions of the fixed parameters.

The design objective of this study was to optimize the proposed MRF brake such that the maximum possible brake toque is achieved while maintaining minimal dimensions (i.e., minimum volume). Accordingly, magnetic analysis software was used for the design optimization process. A simulation model of the proposed brake was developed, and design variables were included. Three major design variables, namely pole width, magnetic channel thickness, and fluid work area, were considered for the optimization process. This is because magnetic flux generation depends on the pole width and current, the flux flow depends on the channel thickness, and the shear stress and output braking torque depend on the fluid work area.

First, the effects of the magnetic channel thickness on the path of the magnetic field lines were determined. If the magnetic channel thickness is excessively small, the channel easily reaches magnetic saturation, which influences the torque efficiency. By contrast, if the thickness is excessively large, the magnetic path becomes excessively long, which results in an unnecessary and excessive volume and weight. Therefore, this study analyzed the magnetic flux density in a channel by setting different channel thicknesses, with the thickness being increased at 1-mm steps. The permeable limit for channel thickness is 5–11 mm. For this study simulations, the pole width, fluid work area, and current were set to 16 mm, 1810 mm^2, and 300 AT, respectively.

Fig. 5(a) presents the simulation results obtained when the magnetic channel thickness was set to 5 mm, revealing the occurrence of magnetic saturation at the corners (magenta); the magnetic field was not sufficiently transferred. Therefore, the channel thickness should be increased. Fig. 5(b) presents the simulation results derived when the magnetic channel thickness was set to 11 mm, representing the maximum possible thickness. In this magnetic channel, the saturation problem was resolved; however, the field path was excessively large.

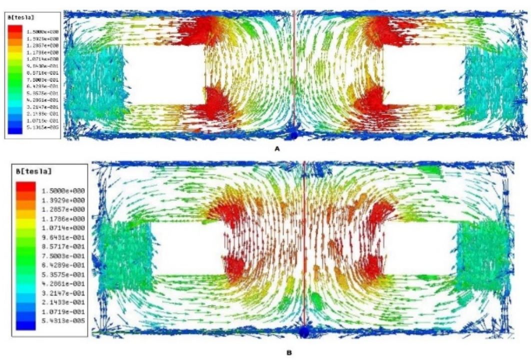

Fig. 5. Distribution of magnetic flux density for the channel thicknesses of (a) 5 and (b) 11 mm.

Fig. 6 presents a graph of the braking torque output for different channel thicknesses. The torque increased considerably with the channel thickness. However, after the thickness reached 8 mm, the torque curve became nearly horizontal. Therefore, considering the brake size and weight, the optimal channel thickness was determined to be 6–10 mm.

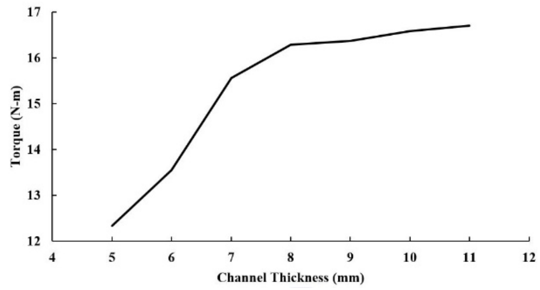

Fig. 6. Effects of magnetic channel thickness on the braking torque.

Second, the effects of the width of the magnetic pole on magnetic efficiency were investigated. Simulations were conducted for different pole widths (ranging from 13 to 19 mm). For the simulations, the magnetic channel thickness was set to 8 mm, fluid work area was set to 1810 mm^2, and current range was set to 180–420 AT (depending on the space available for coil winding). Fig. 7(a) illustrates the results obtained when the pole width was set to 13 mm, indicating substantial magnetic field saturation (magenta), which caused insufficient magnetic field transfer. Therefore, the thickness of the magnetic path must be increased further. However, as displayed in Fig. 7(b), the magnetic field density of the magnetic pole decreased substantially when the pole width was 19 mm at the possible current input. This is because large pole widths occupied the space of the coil winding, causing a reduction in input ampere turns and thus an inadequate overall magnetic field density. Fig. 8 shows the influence of pole width on torque. According to these results, the optimization boundary for the pole width should be 14–18 mm.

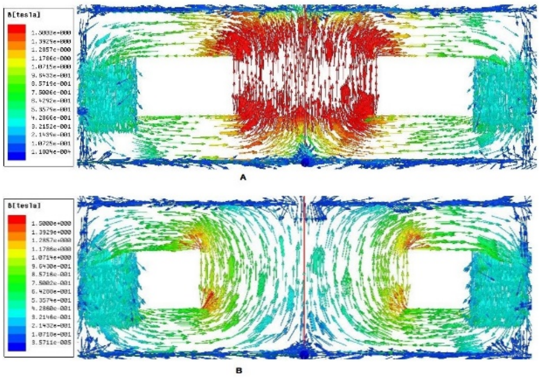

Fig. 7. Distribution of magnetic flux density for the pole width of (a) 13 and (b) 19 mm.

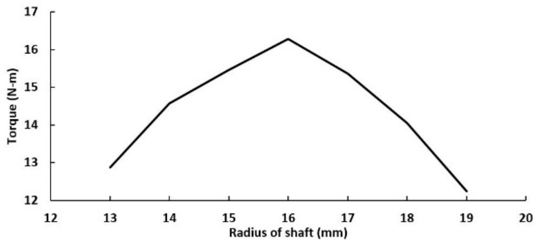

Fig. 8. Effect of the pole width on the braking torque.

Finally, this study investigated the working area of fluid: that is, the area of the single MRF layer located between the rotor and stator plates. The area typically depends on the sizes of the stator and rotor plates. The outer diameters of the stator and rotor plates were fixed; therefore, to change the working area, the inner diameters were altered. “Working area” is used herein for simplicity and to facilitate comprehension. A larger working area results in a stronger total torque effect. However, a large working area reduces the coil-winding space for several ampere-turns. For the study simulation, the working area was set to the range from 1178 to 2384 mm^2. Furthermore, the magnetic channel thickness was set to 8 mm, pole width was set to 16 mm, and current range was set to 180–420 AT (depending on the space available for coil winding). Fig. 9(a) presents the simulation results obtained when the fluid working area was 1178 mm^2. The flux accumulated at poles, and the magnetic field was not sufficiently transferred to the working area. Therefore, the working area must be increased further to increase the field distribution. Fig. 9(b) displays the simulation results obtained when the fluid working area was 2384 mm^2. The problem of flux accumulation at poles was solved because of the increased working area. However, the magnetic flux available at the magnetic pole decreased because the increased working area reduced the coil winding area.

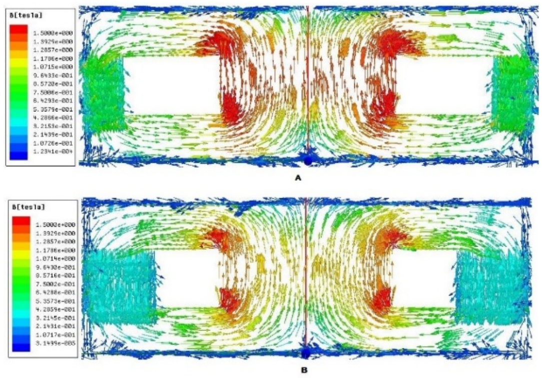

Fig. 9. Distribution of magnetic flux density for the fluid working area of (a) 1178 and (b) 2384 mm^2.

Fig. 10 illustrates the effects of working area on the output torque. The simulation results indicated that when the working area was from 1178 to 1810 mm^2, the profile slope was in the upward direction. However, when the working area exceeded 1810 mm^2, the output torque decreased considerably because of coil area reduction. Therefore, to achieve optimized simulation boundaries, the working area must be within 1395–2007 mm^2.

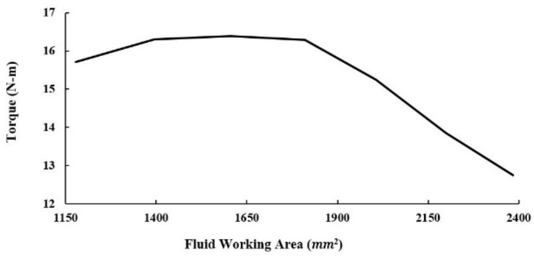

Fig. 10. Effect of the fluid work area on the braking torque.

Table 1. Values or ranges of design parameters.

Fixed parameters		Variable parameters	
Name	Value	Name	Range
MR layer thickness	0.5 mm	magnetic channel thickness	6 mm to 10 mm
plate thickness	1 mm	pole width	14 mm to 18 mm

Stator plates outer diameter	40 mm	coil ampere-turns	180 AT to 460 AT
Number of rotor/stator plates	4/5	fluid work area	2007-1395 mm^2

Parameter optimization

The magnetic pole width, magnetic channel thickness, fluid working area, and coil ampere-turns are most likely to influence the output torque of a brake system. These parameters influence one another or other parameters. As mentioned, the objective of the optimization in this study was to obtain the highest output torque with minimum volume. Accordingly, the most appropriate values of these parameters must be identified. Before the optimization process, the boundary values of the parameters must be defined. The third column of Table 1 presents the design variables and their dimensional ranges. A sequential nonlinear programming (SNLP) optimizer was used. Fig. 11 illustrates the effect of design variables on torque. The horizontal axis of the plot indicates the number of iterations, representing the number of combinations of design variables; a total of 645 combinations were considered in the study. The vertical axis indicates the corresponding output torque. The results revealed that design variables substantially influenced the observed torque. The torque varied between 10 and 17 N·m. Because the objective was to derive the maximum output torque, the maximum possible torque (i.e., 16.955 N·m) was selected. The second column of Table 2 presents the maximum possible torque and corresponding parameter dimensions.

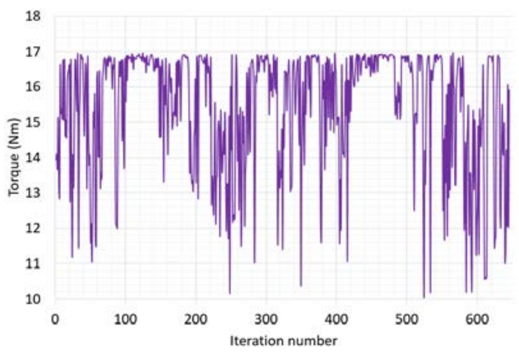

Fig. 11. Effect of design variables on the torque (SNLP results).

Fig. 12 displays the magnetic flux density for the final design, indicating that the magnetic pole and path were close to saturation without being oversaturated. The following section presents a prototype of the proposed brake as well as the results of experiments conducted on this prototype to determine its torque.

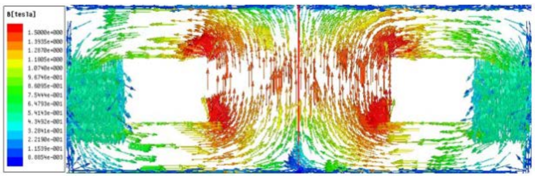

Fig. 12. Distribution of magnetic flux density in the optimized design model.

Table 2. Optimal and prototype dimensions of the designed brake.

Name of the parameter	Optimization results	Prototype dimensions
Torque	16.955 Nm	16.28 Nm
Magnetic channel thickness	9.85 mm	8.50 mm
Pole width	15.65 mm	15.5 mm
Coil ampere-turns	363 AT	300 AT
Fluid work area (single layer)	1559.59 mm^2	1809 mm^2

EXPERIMENTAL TEST

This section presents the experimental validation of the proposed MRB. Because of the limited thickness and available radial space, the magnetic channel thickness and fluid work area were reduced and increased, respectively. In addition, because of the gaps between the coil turns (caused by manual winding) and the maximum current restriction of copper wires, the coil ampere-turns were limited to 300 AT. The third column of Table 2 indicates the optimal possible dimensions of the prototype and the corresponding simulation torque. Because the brake output torque did not decrease substantially, the prototype of the proposed MRB was fabricated using these dimensions. Fig. 13 illustrates the components of the proposed MRB: the lower cover, the magnetic pole, the upper and lower magnetic channels, four rotors, three stators, four rotor plates, three stator contact prevention guides, the magnetic coil, and the housing.

Fig. 14 presents the assembled MBR with a diameter, thickness, and weight of 96 mm, 32 mm, and 1.3 kg, respectively.

Fig. 13. Components of the proposed MRB.

Fig. 14. Prototype of the proposed MRB.

Dynamic Test Platform

Fig. 15 shows the layout of the test platform used in this study. A servomotor was used to rotate the rotor; speed and torque sensors were used to determine the rotor speed and torque available in the MRB, respectively. A control device was used as a current amplifier to supply an exact current to the brake. A MyRIO-1900 card served as the data acquisition system to receive signals from the speed and torque sensors as well as to send a control signal to the MRB.

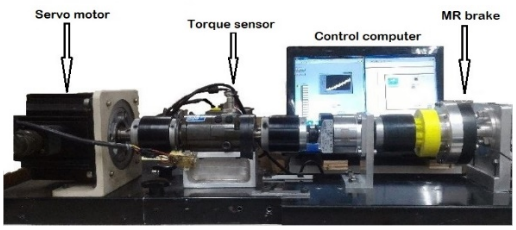

Fig. 15. Test platform for MRF-based brake.

This study conducted tests for the static and dynamic conditions of the MRB. The static tests were conducted to investigate static torques under various currents at different speeds, with the input current corresponding to each speed being varied from 0 to 2 A. The test steps are outlined as follows: First, at zero current, the rotation speed was set to 10 rpm, and the prototype was rotated for 10 min to spread the MRF present inside the MRB evenly throughout the mechanism. Subsequently, the input current was increased from 0 to 2 A at a rate of 0.1 A per pitch, and each pitch was maintained for 15 s. When the maximum current was reached, a waiting period of 15 s was provided to stabilize the torque at 0.1 A; to execute the next pitches, the input current was reduced from 2 to 0 A, and each pitch was maintained for 15 s. The same steps were followed for the tests conducted at rotation speeds of 10, 20, 30, and 100 rpm. The dynamic tests were conducted to determine the brake response and settling time. In this test, a stepped input current was provided, and torque transience was measured during each current step.

Results and discussion

Fig. 16 presents torque outputs obtained from the MRB at different input currents, and these were compared with the simulation results. At zero current, the MRB exhibited a default torque of approximately 0.5 N·m, which can be attributed to the zero field and frictional torques. At the maximum input current (i.e., 2 A), the MRB provided a torque of 12.5 N·m. At all input currents, the experimental values were little lower i.e. approximately 80% of the simulation values. This difference can be attributed to factors such as the production tolerances of the components, coil winding, magnetic pole gap, and assembly of each gap.

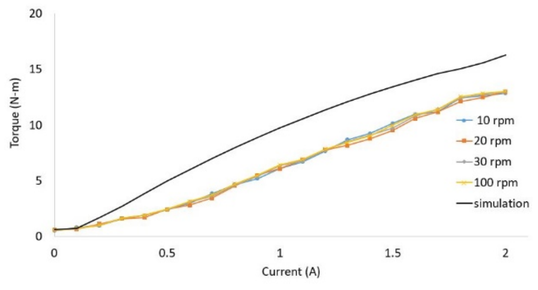

Fig. 16. Experimental and simulation results of proposed MRB at different input currents.

When a magnetic field is applied to a ferromagnetic material such as iron, its atomic dipoles align themselves with the magnetic field. Even when the field is detached, a portion of alignment is retained.

This phenomenon is called material hysteresis.

	Lord MRB (Attia, 2017)	multipole single drum (Shiao, 2013)	multipole bilayer (Shiao, 2016)	proposed MRB
radius (cm)	4.83	7.0	5.0	4.7
length (cm)	5.87	9.8	13.6	4.0
torque (Nm)	5	19.9	27.5	13
TVR (Nm/dm^3)	11.6	13.1	25.8	**46**
time response (ms)	-	250	105	170

Studying this phenomenon is crucial for achieving accurate brake control. Fig. 17 shows the braking torques acquired during activation and deactivation. Between these two paths, a difference of 1.2 N·m was obtained; this can be attributed to the hysteresis in the core and MR layers. However, this difference was not very significant compared with the braking torque. Therefore, this brake can be used as a variable resister in AKO devices.

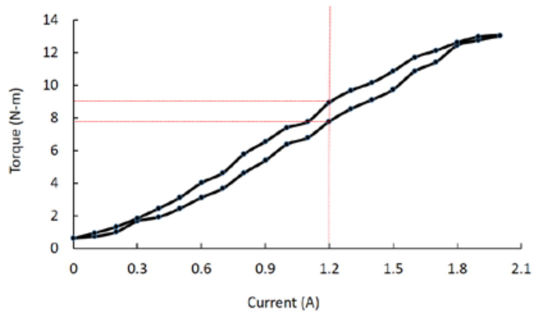

Fig. 17. Hysteresis loop of the MRB.

To understand the speed performance of the proposed MRB, this study analyzed its time response. Fig. 18 presents the response rates of the MRB (i.e., the torque reaction with input current activation and deactivation). The response of the MRB was rapid during brake activation; that is, the rising reaction time was approximately 171.68 ms, and the settling reaction time was approximately 342.33 ms. Furthermore, during deactivation, the rising and settling reaction times were approximately 139.49 and 244.78 ms, respectively. Because of these short reaction times, the proposed MRB can easily achieve torque control. Moreover, this brake is effective at high speed and in active control applications.

Table 3. Comparison of the proposed MRB with existing MRBs.

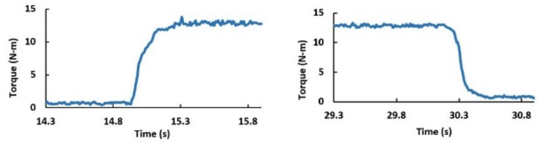

Fig. 18. Response rates during activation and deactivation.

The experimental results indicated that the TVR of the proposed MRB was approximately 46.231 N·m/dm^3, which is substantially higher than that of a commercial LORD rotary brake (14.8 N·m/dm^3). Moreover, the dynamic test results revealed that the response time of the proposed brake was extremely short, and the overall weight of an AKO including this brake was only 2.3 kg, which is much lower than that of a LORD rotary brake–based AKO (4.1 kg). Therefore, the proposed MRB is highly reliable for small-scale engineering and biomedical applications.

Because this brake was designed for AKOs, the primary design objective of this brake was to maximize torque while maintaining minimal dimensions. Few existing MRBs were used as a reference to understand the statistics. The maximum torque, TVR, and response time of the studied MRBs were compared with those of the proposed MRB (Table 3). The proposed brake attained a higher TVR than the existing MRBs did, signifying that the device size required for this MRB to achieve maximum torque is considerably smaller that required by the existing MRBs. Despite its slightly longer response time, the proposed MRB is sufficiently suitable for prosthetic applications. The comparison results demonstrate that the designed brake is more suitable for knee orthosis applications than existing brakes. Fig. 19 displays the real-time application of an AKO embedded with the proposed MRB. The AKO comprises the MRB, a reducer gear, a supporter, and the overall brake structure.

Fig. 19. AKO with the proposed MRB.

CONCLUSIONS

This study designed and tested a novel multilayer MRB for AKO applications. The proposed MRB comprises multiple rotors and stators, which are separated with MRF. The dimensions of the magnetic channel and MRF area were optimized through electromagnetic analysis simulations. A prototype of the designed brake was manufactured for experimental analysis. Through a standard experimental setup, this study examined the real-time performance of the brake. The results indicate that the proposed MRB can provide a torque of 12.5 N·m at a high TVR. The proposed MRB can overcome hysteresis problems with a 1.2-N·m difference, and it can achieve considerably rapid response. Therefore, this brake is highly suitable for AKO applications.

ACKNOWLEDGMENT

This work was financially supported by National Taipei University of Technology and Taipei Medical University. (Project numbers: NTUT-TMU-103-04 and USTP-NTUT-TMU-104-08).

REFERENCES

Ahmadkhanlou, Farzad, Jamaal L. Zite, and Gregory N. Washington. “A magnetorheological fluid-based controllable active knee brace,” Industrial and Commercial Applications of Smart Structures Technologies. Vol. 6527. International Society for Optics and Photonics, (2007).

Arteaga, Oscar, et al. “Design of Human Knee Smart Prosthesis with Active Torque Control,” International Journal of Mechanical Engineering and Robotics Research 9.3 (2020).

Attia, E. M., et al. “Theoretical and experimental study of magneto-rheological fluid disc brake,” Alexandria Engineering Journal, 56.2, 189-200 (2017).

Banala, Sai K., Alexander Kulpe, and Sunil K. Agrawal. “A powered leg orthosis for gait rehabilitation of motor-impaired patients,” Proceedings 2007 IEEE International Conference on Robotics and Automation. IEEE (2007).

Beyl, Pieter, et al. “Mechanical design of an active knee orthosis for gait rehabilitation,” 2007 IEEE 10th International Conference on Rehabilitation Robotics. (2007).

Carlson, J. David, Wilfried Matthis, and James R. Toscano. “Smart prosthetics based on magnetorheological fluids,” Smart structures and materials 2001: industrial and commercial applications of smart structures technologies. Vol. 4332. International Society for Optics and Photonics, 2001.

Data, L. T. “MRF-140CG Magneto-Rheological Fluid,” LORD Corp. 48 (2008)

Dollar, Aaron M., and Hugh Herr. “Active orthoses for the lower-limbs: challenges and state of the art,” 2007 IEEE 10th International Conference on Rehabilitation Robotics (2007).

Gao, Fei, Yan-Nan Liu, and Wei-Hsin Liao. “Optimal design of a magnetorheological damper used in smart prosthetic knees,” Smart Materials and Structures 26.3: 035034, (2017).

Josep M. Font-Llagunes, Rosa Pàmies-Vilà, Javier Alonso and Urbano Lugrís, “Simulation and design of an active orthosis for an incomplete spinal cord injured subject,” ScienceDirect, Procedia IUTAM 2, pp.68-81(2011).

Li C, Tokuda M, Furusho J, Koyanagi KI, Morimoto S, Hashimoto Y, Nakagawa A, Akazawa Y. “Research and development of the intelligently-controlled prosthetic ankle joint,” IEEE 2006 International Conference on Mechatronics and Automation, pp. 1114-1119 (2006).

Li, W. H., and H. Du. “Design and experimental evaluation of a magnetorheological brake,” The International Journal of Advanced Manufacturing Technology, 21.7, 508-515 (2003).

Ma, Hao, et al. “Design and testing of a regenerative magnetorheological actuator for assistive knee braces,” Smart Materials and Structures 26.3:

035013, (2017).

Nguyen, Q. H., and S. B. Choi. "Optimal design of a novel hybrid MR brake for motorcycles considering axial and radial magnetic flux," Smart Materials and Structures, 21.5, 055003 (2012).

Nguyen, Q. H., V. T. Lang, and S. B. Choi. "Optimal design and selection of magneto-rheological brake types based on braking torque and mass," Smart Materials and Structures, 24.6, 067001 (2015).

Pratt, Jerry E., et al. "The RoboKnee: an exoskeleton for enhancing strength and endurance during walking," IEEE International Conference on Robotics and Automation, Proceedings. ICRA'04. 2004. Vol. 3 (2004).

Rabinow J. "The magnetic fluid clutch. Electrical Engineering," Dec; 67(12):1167 (1948).

Rosensweig RE, Kaiser R, Miskolczy G. "Viscosity of magnetic fluid in a magnetic field," Journal of Colloid and Interface Science. 1969 Apr 1;29(4):680-6 (1969).

Shiao, Yaojung, and Quang-Anh Nguyen. "Development of a multi-pole magnetorheological brake," Smart Materials and Structures 22.6, 065008 (2013).

Shiao, Yaojung, Nguyen Anh Ngoc, and Chien-Hung Lai. "Optimal design of a new multipole bilayer magnetorheological brake," Smart Materials and Structures 25.11, 115015 (2016).

Takesue N, Asaoka H, Lin J, Sakaguchi M, Zhang G, Furusho J. "Development and experiments of actuator using MR fluid," 26th Annual Conference of the IEEE Industrial Electronics Society, IECON (2000).

Wang, Daoming, and Youfu Hou. "Design and experimental evaluation of a multidisk magnetorheological fluid actuator," Journal of intelligent material systems and structures 24.5, 640-650 (2013).

Weinberg, Brian, et al. "Design, control and human testing of an active knee rehabilitation orthotic device," Proceedings 2007 IEEE International Conference on Robotics and Automation. (2007).

Wu, Jie, et al. "Design, simulation and testing of a novel radial multi-pole multi-layer magnetorheological brake," Smart Materials and Structures 27.2, 025016 (2018).

Zhou, Wei, Chee-Meng Chew, and Geok-Soon Hong. "Development of a compact double-disk magneto-rheological fluid brake," Robotica 25.4, 493-500 (2007).